5-1-1998

# Holographic Microscope for Measuring Displacements of Vibrating Microbeams Using Time-Averaged, Electro-Optic Holography

Gordon C. Brown

Ryszard J. Pryputniewicz
*Worcester Polytechnic Institute*, rjp@wpi.edu

# Holographic microscope for measuring displacements of vibrating microbeams using time-averaged, electro-optic holography

**Gordon C. Brown,** MEMBER SPIE
**Ryszard J. Pryputniewicz,** FELLOW SPIE
Worcester Polytechnic Institute
Center for Holographic Studies and Laser $\mu$mechaTronics
Mechanical Engineering Department
Worcester, Massachusetts 01609-2280
E-mail: gcbrown@wpi.edu

**Abstract.** An optical microscope, utilizing the principles of time-averaged hologram interferometry, is described for microelectromechanical systems (MEMS) applications. MEMS are devices fabricated via techniques such as microphotolithography to create miniature actuators and sensors. Many of these sensors are currently deployed in automotive applications which rely on, or depend on, the dynamic behavior of the sensor, e.g., airbag sensors, ride monitoring suspensions sensors, etc. Typical dimensions of current MEMS devices are measured in micrometers, a small fraction of the diameter of a human hair, and the current trend is to further decrease the size of MEMS devices to submicrometer dimensions. However, the smaller MEMS become, the more challenging it is to measure with accuracy the dynamic characteristics of these devices. An electro-optic holographic microscope (EOHM) for the purpose of studying the dynamic behavior of MEMS type devices is described. Additionally, by performing phase measurements within an EOHM image, object displacements are determined as illustrated by representative examples. With the EOHM, devices with surface sizes ranging from approximately $35\times400$ to $5\times18$ $\mu$m are studied while undergoing resonant vibrations at frequencies as high as 2 MHz.  [S0091-3286(98)00505-4]

Subject terms: microelectromechanical systems; electro-optic holographic microscope; microscopic holography; electro-optic holography; microsensors; hybrid methods; automotive applications.

Paper CAR-05 received Nov. 10, 1997; accepted for publication Dec. 5, 1997.

## 1 Introduction

With the advent of microelectromechanical systems (MEMS), new test methods are being developed to handle the unique challenges that these microdevices pose to current test methods. This paper describes the development of an electro-optic holographic microscope (EOHM), an optical instrument that is capable of (1) imaging MEMS devices and (2) the interferometric determination of mode shapes using time-averaged holography. Current studies of vibrating cantilever microbeams using the EOHM indicate that this system can resolve objects with nominal dimensions as small as $5\times18$ $\mu$m. The scope of this paper encompasses a description of the microscope and techniques and presentation of preliminary results and their relationship to future results.

In certain devices, the trend of electronic and mechanical design and manufacturing studies requires decreasingly smaller and smaller external packaging, which in turn, has called for even smaller internal components. Many of these components are miniature replicas of much larger ones, only designed to operate on a much smaller scale. Replicas of gears, motors, and sensors are being manufactured with nominal dimensions measured in micrometers. These replicas are known as microelectromechanical devices (MEMD), and combining the functions of two or more devices creates a system, or an MEMS.

MEMS are a specific collection of MEMD. These devices are micrometer-sized mechanisms typically manufactured using very large scale integration (VLSI) techniques adopted from the microelectronics industry and are used in sensor and actuator applications. This process enables not only the fabrication of the MEMS mechanical structure, but also enables its direct integration with microelectronics, thus providing the essential electrical conduit to the real world for operating power and control. Engine blocks equipped with integrated sensors for monitoring pressure, temperature, and flow conditions from within; suspension systems outfitted with embedded vibration control sensors for improved handling and ride control; and tires constructed with molded-in pressure and temperature sensors are just a few examples of MEMS applied in the automotive industry. Now, imagine coupling these microsensors and controllers to certain materials whose properties of stiffness, shape, and color are alterable via temperature or photoelectric effects; for example; MEMS will, quite profoundly, change the way we currently engineer and use our automotive products.

Several techniques are used to manufacture MEMS devices; most are based on the photolithographic process. Basically, each begins with a block of base material, typically $\langle100\rangle$ silicon, to which material is added or etched away using premade mask patterns laid over the base material. Added material can be almost anything from more silicon,

 0091-3286/98/$10.00 

to various metals such as aluminum or gold, and even polyimides. Then these different layers of material can be etched away or built up to create various devices such as atomic force microscope (AFM) sensors. AFM sensors are readily available and, for this paper, are convenient and effective objects for demonstrating the EOHM.

The AFM probe tip is one example of a MEMS type sensor used to characterize material surfaces. This is accomplished by tracking a resonating sensor just nanometers above the material surface and recording changes in its resonant behavior. The resonant changes in the sensor occur due to changes in van der Waals forces on the surface of the material as a function of height, e.g., surface roughness. By recording the AFM's response, surface measurements are obtained.

As with all tools or devices manufactured on scales of any size, these microdevices must be tested to validate their performance. Techniques such as laser vibrometry have been developed that enable determination of amplitude at resonance, and they work quite well while providing pointwise mapping of the object. Yet, pointwise mapping is time consuming and requires a ''steady state'' condition during the entire period of data acquisition, which can be quite long. However, holographic interferometry is not only noninvasive but is a whole-field imaging technique and provides results in near real time. This, we believe, is an advantage over pointwise scanning techniques.

It is essential that computer analysis be integrated with experimental work. First, experimental techniques can be both expensive and time consuming, and second, and perhaps most important, redesign or optimization of componentry is not practical through experiment alone. The finite element method (FEM) has proven to be an effective analysis tool when given reliable data from experiment. Material properties, loading conditions, boundary conditions, and geometry validated through experiment are used as input for the FEM analysis. Once the experimental data are integrated into the FEM, a designer can begin optimizing the model for the desired quantity, e.g., mode shape or resonant frequency.

In this paper, we utilize the EOHM to investigate the dynamic characteristics of AFM probe tips and develop an FEM model based on the experimental data. With the EOHM presented in this paper, MEMS devices with nominal dimensions of 450 to 20 $\mu$m were studied.

## 2 Analytical Considerations

### 2.1 *Description of the Objects Studied*

In this paper, two 2.7-$\mu$m-thick silicon cantilever microbeams were studied. The microbeams have a nearly constant trapezoidal cross section; one such microbeam is pictured in Fig. 1(a), with dimensions shown in Fig. 1(b). Dimensions were measured using Nikon MM-11 Measurescope and Measuregraph software with 0.5-$\mu$m accuracy. Thickness measurements were made in the scanning electron microscope (SEM).

### 2.2 *Determination of Resonant Frequency and Mode Shape*

In this analysis, we assume that the microbeam's material is homogeneous, isotropic, and that it obeys Hooke's law.

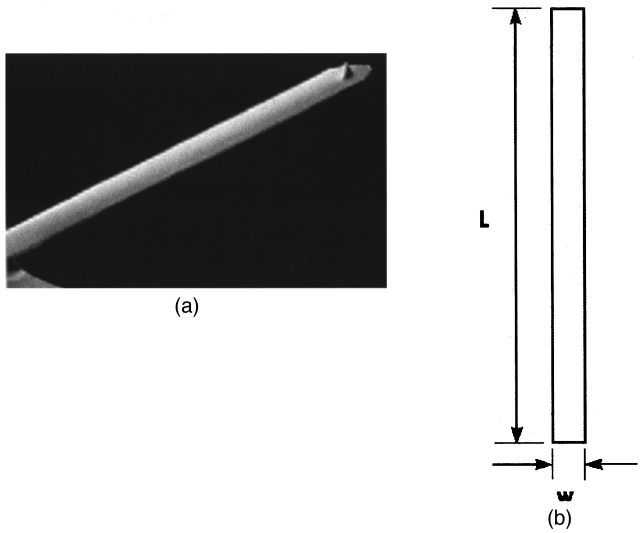


**Fig. 1** Trapezoidal cross section microbeam: (a) SEM micrograph and (b) characteristic dimensions. Here, $L=450$ $\mu$m, 225 $\mu$m; $w=25.3$ $\mu$m; and microbeam thickness $t=2.7$ $\mu$m.

The microbeam is also assumed to be straight, of uniform cross section, and undergoing small transverse deflections. Considering these assumptions and using Euler beam theory, we can obtain an equation relating resonant frequency to the microbeam's material properties and geometry as[1]

$$\omega_n=\frac{(\beta_n)^2}{L^2}\left(\frac{EI}{\rho A}\right)^{1/2}, \tag{1}$$

where $\omega_n$ is the $n$'th resonant frequency (in bending); $E$ is the elastic modulus of the material; $I$ is the area moment of inertia; $\rho$ is the material density; $A$ is the cross-sectional area; $L$ is the length; and $\beta_n$ is a parameter determined by the boundary conditions for the $n$'th mode of vibration, and for the first eight bending modes has the values[1] 1.87510, 4.69409, 7.855, 10.996, 14.137, 17.279, 20.420, and 23.562, respectively.

Additionally, the equation that describes the mode shape at resonance is of the form[1]

$$z_n(y)=\left[\cos h\left(\frac{\beta_n}{L}y\right)-\cos\left(\frac{\beta_n}{L}y\right)\right]+\left[\sin h\left(\frac{\beta_n}{L}y\right)-\sin\left(\frac{\beta_n}{L}y\right)\right], \tag{2}$$

where $z(y)$ is the out of plane deflection of the microbeam, and $y$ is the position along the microbeam's length.

## 3 Computational Considerations—FEM

The FEM is quite suited for solving problems of a dynamic nature that are governed by the equation

$$\mathbf{M}\{\ddot{\mathbf{u}}\}+\mathbf{C}\{\dot{\mathbf{u}}\}+\mathbf{K}\{\mathbf{u}\}=\{\mathbf{F}(t)\}, \tag{3}$$

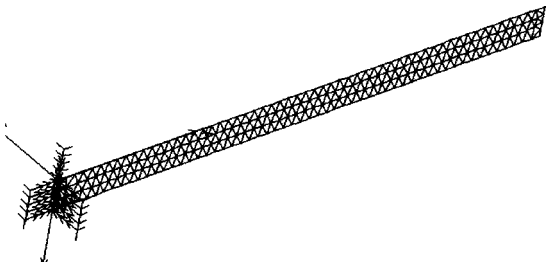

**Fig. 2** Finite element model of the trapezoidal cross section microbeam: eight-noded shell elements.

where **M** is the total mass matrix of the structure; **C** is the structural damping matrix; **K** is the stiffness matrix; $\{\ddot{\mathbf{u}}\}$, $\{\dot{\mathbf{u}}\}$, and $\{\mathbf{u}\}$ are the nodal accelerations, velocities, and displacements, respectively; and $\{\mathbf{F}(t)\}$ is the vector of applied time-varying forces.

One of the most prominent and frequently performed types of dynamic analysis deals with the prediction of natural frequencies and corresponding mode shapes of undamped structures under free vibrations; this is the so-called eigenvalue problem. For the modal analysis, or eigenvalue problem, Eq. (3) reduces to

$$\mathbf{M}\{\ddot{\mathbf{u}}\}+\mathbf{K}\{\mathbf{u}\}=0, \tag{4}$$

which indicates that there is no damping and $\mathbf{C}=0$.

If a sinusoidal vibration is assumed, then we can write

$$u=A\cos(\omega t), \tag{5}$$

and

$$\ddot{u}=-A\omega^2\cos(\omega t)=-\omega^2 u, \tag{6}$$

where $A$ is the amplitude of vibration, $\omega$ is the angular frequency of the vibration, and $t$ is time. Substituting Eqs. (5) and (6) into Eq. (4), we obtain

$$(\mathbf{K}-\omega^2\mathbf{M})\{\mathbf{u}\}=0, \tag{7}$$

where $\omega^2$ and $\{\mathbf{u}\}$ are unknowns; $\omega^2$ represents the eigenvalue; and $\{\mathbf{u}\}$ is the normalized eigenvector, which describes the corresponding mode shape.

Reliable and accurate application of the FEM requires validation of the model used to represent the object under study. Model validity is influenced primarily by the geometry of the object, its material properties, the applied loading conditions, and the constraint conditions imposed on the object. Finite element models of the microbeams were meshed using eight-noded shell elements with six degrees of freedom at each node (i.e., three translations and three rotations). The FEM meshed geometry for the microbeam used in this study is shown in Fig. 2.

## 4 Experimental Investigation

In general, experimental verification of resonant frequencies requires real-time, whole-field analysis of the vibrating objects being studied, and ''conventional'' electro-optic holography (EOH) satisfies both of these requirements. In studying MEMS behavior,[2] however, there is the additional requirement of imaging very small objects, microbeams, for example. The EOH system must be able to image objects having typical dimensions ranging from 450 to 10 $\mu$m. Following is a description of the EOHM system to image microbeams of this size.

### 4.1 *Description of the EOHM*

The schematic of the EOHM system described in this paper is shown in Fig. 3. In this system, the laser output is di-

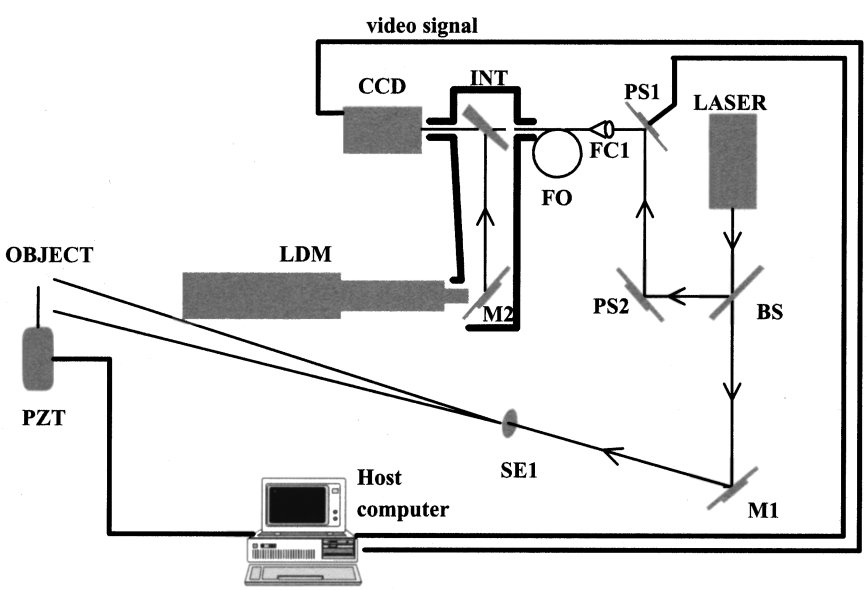


**Fig. 3** Optical configuration of the EOHM system used in this study: INT, interferometer; BS, beamsplitter; *M*1 and *M*2, mirrors; PS1 and PS2, phase stepper/mirror assemblies; SE1, spatial filter beamexpander assembly; FC1, fiber optic coupler; FO, fiber optic link; PZT, electromechanical exciter; LDM, long distance microscope lens; and CCD, imaging camera.

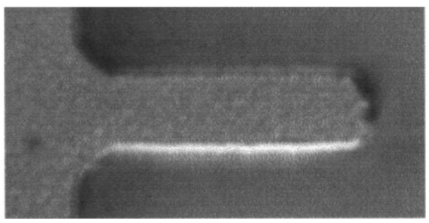

**Fig. 4** Photograph of the 5-×18-$\mu$m beam.

vided into two beams via beamsplitter (BS). One of these beams is directed by mirror $M1$ through the beamexpander (SE1) to uniformly illuminate the object; that is the object beam. The other beam, the reference beam, is directed to the reference port of the interferometer (INT) by means of a mirror affixed to the phase steppers PS1 and PS2, and is coupled via fiber optic coupler FC1 into an optical fiber (FO). Phase steppers PS1 and PS2 can be driven piezoelectrically to introduce phase steps between consecutive frames. The reference and object beams are then collected and combined by the interferometer and then directed toward the CCD imaging camera. The detected image is then sent to the image processor, and finally to the viewing monitor.

This EOHM is unique because of the long-working-distance microscope (LDM) incorporated into the interferometer. This microscope has three major components: (1) primary objective lens, (2) internal focusing system (including a 2.1× zoom module), and (3) ocular lens.

The microscope lens used in this experiment is an Infinity K2 long-distance microscope lens. The K2 consists of a two-stage objective system, a microscope tube, and an ocular. The objective system has as its components an interchangeable fixed-focus front objective lens, a variable focus rear objective lens, and the 2.1× zoom module. The ocular is interchangeable as well, typically either 10× or 20×. This microscope has a working distance variable from 2 to 6 in., and a numerical aperture (NA) of 0.190. The theoretical resolution of the lens alone is 1.75 $\mu$m, and the smallest resolvable object observed with the EOHM is the 5-×18-$\mu$m microbeam shown in Fig. 4. Using a 5× primary objective lens, a working distance of 4 in. (102 mm), a 20× ocular, a 0.5-in. array CCD camera, and a 13-in. video monitor, the total system magnification approaches 1000×.

Typical microscope objectives have short working distances. With its extraordinarily long working distance, the EOHM provides ample space between the microscope and test objects. This, in turn, enables the microscope to image objects contained within an ''isolation'' chamber. Alternatively, the primary objective could be detached and placed inside of the isolation chamber, while the main body of the lens remains outside of the chamber, viewing the object through an optical window. The current laboratory setup of the EOHM prototype is shown in Fig. 5.

### 4.2 *Time-Averaged Hologram Interferometry*

Displacement measurements of sinusoidally vibrating objects using the EOHM method are made by considering

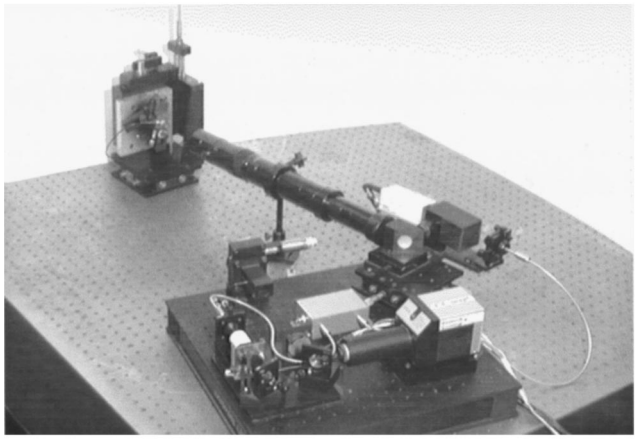

**Fig. 5** Laboratory setup of the EOHM prototype.

time-averaged hologram interferometry.[1–6] In EOHM, the CCD element essentially measures the 2-D intensity distributions, or irradiance profiles, of the overlapping object and reference fields on a frame-by-frame basis. Processing of interferometric data requires measurement of the spatial distribution of irradiances of each frame.

In time-averaged hologram interferometry, a single holographic recording of an object undergoing a cyclic vibration is made. With the exposure time long in comparison to one period of the vibration cycle, the hologram effectively records an ensemble of images corresponding to the time average of all positions of the object while it is vibrating. During the reconstruction of such a hologram, the interference occurs between the entire ensemble of images, with the images recorded near zero velocity (i.e., maximum displacement) contributing most strongly to the reconstruction. The interference fringes observed during the reconstruction of the time-averaged holograms are of unequal brightness. In fact, they are modulated by the square of the zero-order Bessel function of the first kind. Quantitative interpretation of the Bessel fringes is discussed in Refs. 7–12 and yields displacements of objects to within a small fraction of a micrometer.

In general, for a sinusoidally vibrating object the irradiance $I$ seen at the CCD is

$$I = I_a(x,y) + I_m(x,y) J_0^2[|\Omega_t(x,y) - B|], \tag{8}$$

where $I_a$ represents the unmodulated average background irradiance; $I_m$ is the maximum irradiance of the modulated light field; $J_0$ represents the zero-order Bessel function of the first kind; $\Omega_t$ is the time-varying fringe-locus function, which contains phase information of the object displacements; $B$ is the bias modulation imposed on the light beam during recording of the hologram; and $x$ and $y$ represent spatial coordinates. In Eq. (8), $I_a$, $I_m$, and $\Omega_t$ are unknown quantities. When the vibration is sinusoidal, the fringe modulation function is described by the square of the zero-order Bessel function of the first kind. To obtain quantitative information on object displacements, Eq. (8) can be

solved using three frames of irradiance distributions, each with a different bias modulation. Because of the nature of the Bessel function, Eq. (8) cannot be readily solved for $\Omega_t$. However, recognizing the similarity of $(J_0)^2$ to the $\cos^2$ function, we can obtain an approximate solution for the time varying fringe-locus function as follows:

$$\Omega_{t_{\text{approx}}} = \frac{1}{2}\tan^{-1}\left\{\left[\frac{1-\cos 2B}{\sin 2B}\right]\frac{I_3-I_2}{2I_1-I_2-I_3}\right\}, \tag{9}$$

where $I_1$, $I_2$, and $I_3$ are irradiances corresponding to each of the three frames, respectively. Equation (9) gives the wrapped, or modulo $2\pi$ phase, distribution on the studied object. This solution is based on representation of the three irradiances, corresponding to the bias modulation, as

$$I_i = I'_a(x,y) + I'_m(x,y)\cos\left[2\Omega_t(x,y) - 2B_i\right], \quad i = 1,2,3 \tag{10}$$

where

$$I'_a(x,y) = I_a(x,y) + \frac{I_m(x,y)}{2}, \quad I'_m(x,y) = \frac{I_m(x,y)}{2}, \tag{11}$$

$i$ represents the sequential frame order, and the $B_i$ are the values corresponding to zero, positive, and negative bias modulations, respectively. The actual solution of the fringe-locus function can then be obtained by passing the approximate solution through a preconstructed look-up table (LUT).

For the EOHM setup, bias modulation is introduced via a phase-shifting mirror mounted in the reference arm of the interferometer. Both the phase and magnitude of the applied bias must be determined and one method is as follows.[4] First, the bias signal is adjusted so that it is in phase with the vibration of the object, this enables the bias term in Eq. (8) to be a simple additive term within the argument of the Bessel function, as shown in Eq. (8). Second, and without changing phase, the magnitude of the bias is set in such a way that the square of the Bessel function in Eq. (8) equals 0 when the object is stationary (object excitation off, $\Omega_t = 0$). This occurs when, while observing the real-time EOHM image displayed on the monitor, the image becomes black. At this point, $B = 2.4048$, the first zero of the Bessel function. We take this value as the positive bias, and obtain the negative bias by shifting the phase of the positive bias by 180 deg.

### 4.3 *Effect of Speckle Noise*

Speckle noise is typically not a problem with the EOHM configuration. Speckle is a phenomenon associated with the viewing of monochromatic light that is diffusely reflected from the surface of an object and, in part, depends on the wavelength of light used, type of illumination (direct or diffuse), NA of the optical viewing system, and the surface roughness of the object. The size $\delta$ of a speckle formed by an optical system can be described by the following relationship:

**Table 1** Material properties of the AFM probe tips used in this study.

| Material | Density (g/mm$^3$) | Poisson Ratio | Elastic Modulus (GPa) |
|---|---|---|---|
| Si | 2.33 | 0.24 | 140±14 |

$$\delta \propto \frac{\lambda \text{NA}}{\text{SR}D}. \tag{12}$$

Equation (12) shows that speckle size is proportional to wavelength λ and NA, and is inversely proportional to the surface roughness (SR) and diffusivity $D$ of the illuminating light field. For the EOHM, λ, $D$, and NA are constant parameters and speckle size is essentially determined by SR of the object. In the case of the MEMS devices studied in this paper, SR is of the order of nanometers and the speckles formed are so large that the object is essentially specular.

### 4.4 *Experimental Method*

Experimental mode shapes of AFM probe tips were investigated using the EOHM. Basically, the EOHM provides near real-time whole-field visualization of interferometric fringe patterns describing resonant mode shapes. The objects studied for fringe pattern analysis were 450- and 255-$\mu$m, Si AFM tips. All geometry dimensions were measured in an AMR 1610 SEM with integrated video processing software, and the material densities and Poisson ratios were obtained from the manufacturer as listed in Table 1.

Excitation of the silicon AFM tips was achieved by rigidly affixing them to a Steavely 15 MHz piezoelectric transducer (PZT) exciter assembly positioned within the EOHM. The PZT exciter was connected to a Wavetek model 650 waveform synthesizer and operated to induce sinusoidal vibrations in the attached AFM probe tip.

## 5 Results and Discussion

Use of the FEM is essential to predict vibration characteristics of MEMS components being developed. FEM enables us to accurately model a component without the need for extended testing of expensive prototype models. However, results produced by the FEM depend largely on the input information relating to the boundary conditions of the object; loads acting on the object; and the object's material properties, geometry, and discretization.

Finite element (FE) analysis was performed using COSMOS\M software. The models were constructed from eight-noded shell elements with six degrees of freedom at each node. The natural frequencies and mode shapes were then determined by eigenvalue calculations.

For the AFM tips studied, the analytical and FE-predicted mode shapes and frequencies compared to within 3% of the experimental results from the EOHM. The analytical and FE mode shapes and EOHM recorded fringe patterns are shown in Figs. 6 and 7 for the 450- and

225-$\mu$m AFM tips, respectively. Figures 6(a) to 6(f) show the first through sixth bending modes, while Fig. 6(g) shows the eighth bending mode; data for the seventh bending mode are not shown. Maximum displacement amplitudes are about 400 nm, or 75% of the wavelength of laser light used.

Undamped, natural modes of vibration are orthogonal and symmetric. Referring to Fig. 6(e), we see from the EOHM fringe pattern that the fifth bending mode at 632 kHz is nonsymmetric. Although the exact cause of this asymmetry is not certain, damping, whether structural or air resistance related, is suspected to be more significant in this particular mode. Nevertheless, its effect is seen immediately in the distorted fringe pattern of the interferogram.

Figures 7(a) and 7(b) show the FE mode shapes and the EOHM fringe patterns for the first and second bending modes, respectively, for the 225-$\mu$m AFM tip. Maximum amplitudes of displacement for the EOHM images shown are about 1.7 and 1.5 microns for the first and second modes, respectively.

## 6 Conclusions

We have demonstrated the use of an EOHM to determine resonant frequencies and mode shapes of vibrating AFM probe tips by employing the time-averaged holographic method. Additionally, we have demonstrated the ability of the EOHM to identify modes of the vibrating AFM tips. We have also demonstrated that the EOHM can image MEMS type devices as small as $5\times18$ $\mu$m. We further demonstrated the use of the EOHM to identify irregularities of AFM tip geometry by observing differences between the experimentally obtained data and the FE-calculated mode shape of the fifth bending mode.

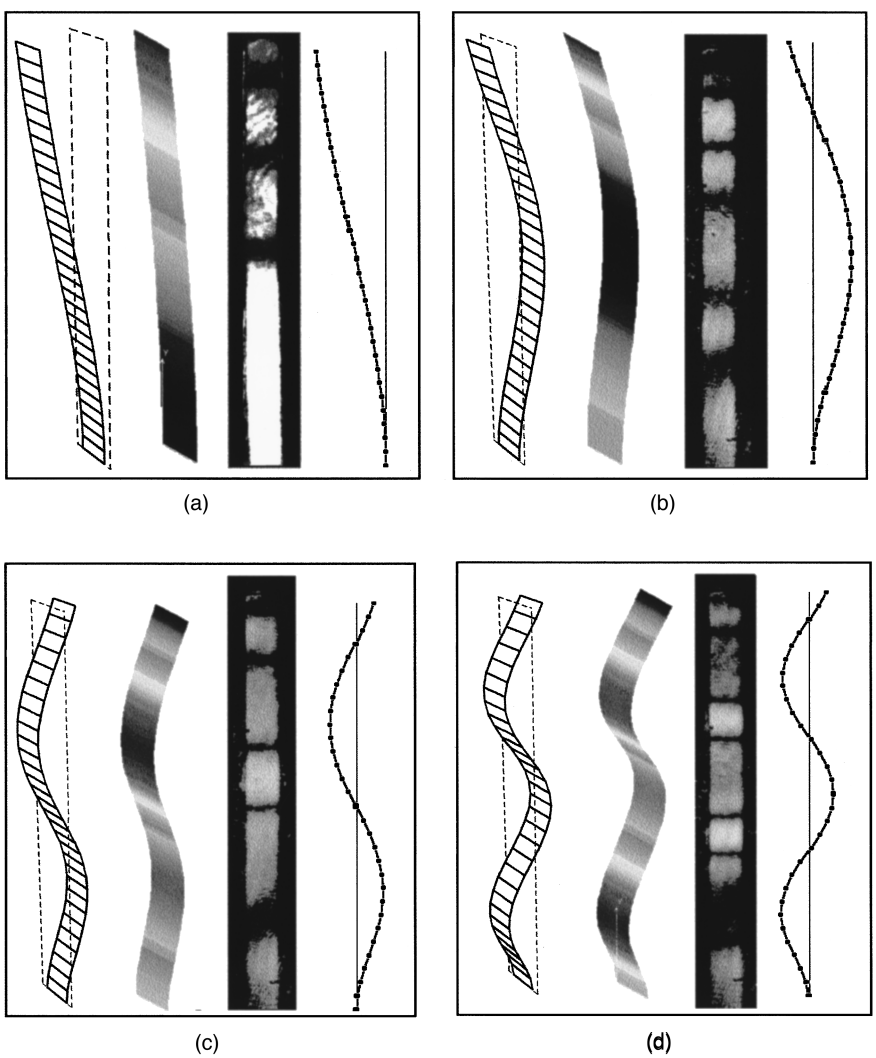


**Fig. 6** Analytical and FE mode shapes, EOHM fringe patterns, and representative experimental displacements for the 450-$\mu$m AFM tips: (a) first bending at 11 kHz, (b) second bending at 63 kHz, (c) third bending at 193 kHz, (d) fourth bending at 381 kHz, (e) fifth bending at 632 kHz, (f) sixth bending at 947 kHz, and (g) eighth bending at 1.8 MHz. Continued on next page.

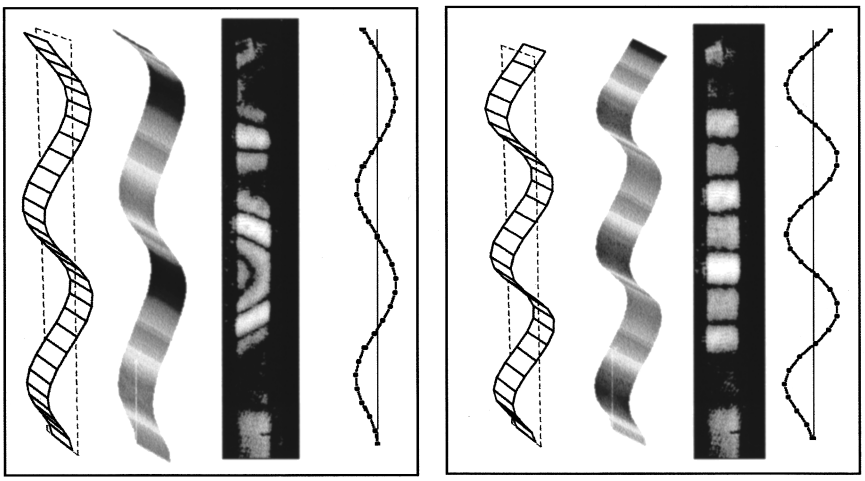

(e) (f)

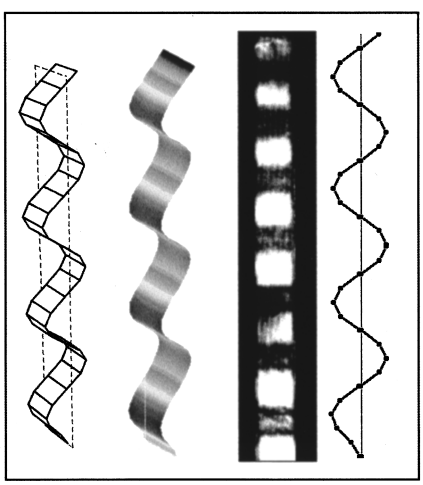

(g)

**Fig. 6** Continued.

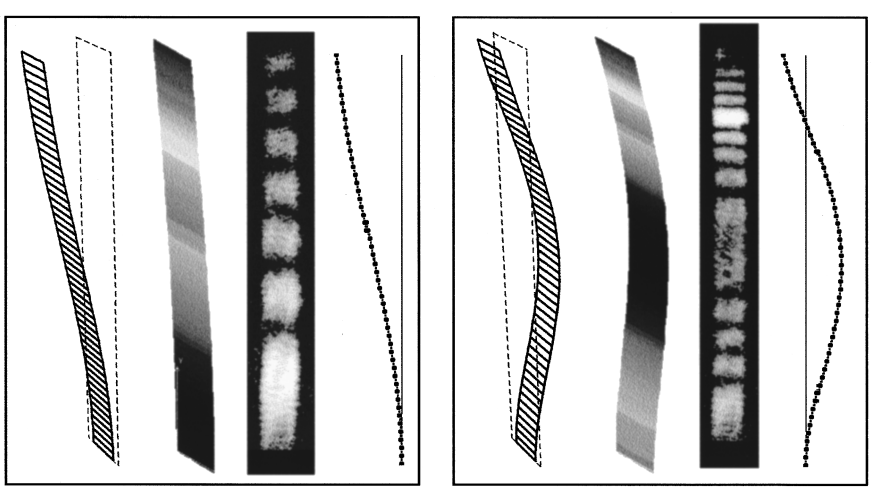

(a) (b)

**Fig. 7** Analytical and FE mode shapes, EOHM fringe patterns, and representative experimental displacements for the 225-$\mu$m AFM tips: (a) first bending at 157 kHz and (b) second bending at 970 kHz.

### *Acknowledgments*

This study was supported by an AASERT grant from ARPA/ESTO, the Advanced Research Projects Agency/ Electronic Systems Technology Office, Arlington, Virginia.

### *References*

1. G. C. Brown and R. J. Pryputniewicz, ''Investigation of submillimeter components by heterodyne holographic interferometry and computational methods,'' *Proc. SPIE* **1755**, 122–130 (1992).
2. G. C. Brown and R. J. Pryputniewicz, ''Experimental and computational determination of dynamic characteristics of microbeam sensors,'' *Proc. SPIE* **2545**, 108–119 (1995).
3. K. A. Stetson and W. R. Brohinsky, ''An electro-optic holography system for vibration analysis and nondestructive testing,'' *Proc. SPIE* **746**, 44–51 (1987).
4. K. A. Stetson and W. R. Brohinsky, ''Fringe-shifting technique for numerical analysis of time-average holograms of vibrating objects,'' *J. Opt. Soc. Am. A* **5**, 1472–1476 (1988).
5. R. J. Pryputniewicz and K. A. Stetson, ''Measurement of vibration patterns using electro-optic holography,'' *Proc. SPIE* **1162**, 456–467 (1989).
6. G. C. Brown and R. J. Pryputniewicz, ''Investigation of a submillimeter cantilever beam of variable cross section by computational and hologram interferometry methods,'' *Proc. SPIE* **1821**, 72–81 (1992).
7. K. A. Stetson, ''Effects of beam modulation on fringe loci and localization in time-average hologram interferometry,'' *J. Opt. Soc. Am.* **60**, 1378–1384 (1970).
8. C. M. Vest, *Holographic Interferometry*, Wiley, New York (1979).
9. R. J. Pryputniewicz, ''Holographic and finite element studies of vibrating beams,'' *Proc. SPIE* **599**, 54–62 (1985).
10. R. J. Pryputniewicz, ''Time-average holography in vibration analysis,'' *Opt. Eng.* **24**, 843–848 (1985).
11. R. J. Pryputniewicz, ''Quantitative holographic analysis of small components,'' *Proc. SPIE* **604**, 71–85 (1986).
12. R. J. Pryputniewicz, ''Quantitative interpretation of time-average holograms in vibration analysis,'' in *Optical Metrology*, O. D. D. Soares, Ed., pp. 296–316, NATO ASI Series E: Applied Sciences, No. 131, Martinus Nijhoff Publishers, Dodrecht (1987).

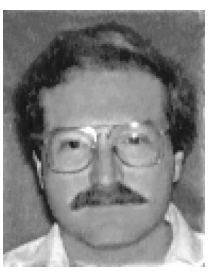

**Gordon C. Brown** is a research assistant for the Center for Holographic Studies and Laser $\mu$mechaTronics at Worcester Polytechnic Institute (WPI). He holds a BS degree in applied geophysics from Michigan Technological University, and a MS degree in mechanical engineering from WPI. He is currently a PhD candidate at WPI, conducting research in holographic interferometry techniques for nondestructive testing of microelectromechanical systems.

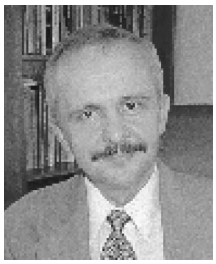

**Ryszard J. Pryputniewicz** was educated both in Poland and the United States. He has been professor of mechanical engineering and founding director of the Center for Holographic Studies and Laser $\mu$mechaTronics (CHSLT) at Worcester Polytechnic Institute (WPI) in Worcester, Massachusetts, since 1978. Previously, he was a faculty member and director of the Laser Research Laboratory at the School of Engineering and the Health Center of the University of Connecticut for 6 years and a member of the Aerospace technical staff for 4 years. His research interests concentrate on theoretical and applied aspects of microelectromechanical systems, smart sensors and structures, and, in particular, holographic interferometry. In this work, he emphasizes unification of analytical, computational, and experimental solution methodologies, especially when they can be merged to provide solutions where none would be obtainable otherwise, to ease the solution procedure, or to attain improvements in the results. He is an SPIE Fellow and a member of Kappa Mu Engineering Honor Society, Pi Tau Sigma, Tau Beta Pi, and Sigma Xi. He received the SPIE Dennis Gabor Award, Ralph R. Teetor National Educational Award of SAE, Young Engineer of the Year National Award, Admiral Earle Award, and the Outstanding Young Man of America, and has been listed in *Who's Who in the East* and *Who's Who in Technology Today*. He has participated in SPIE and SPIE-related activities since 1972. He has been the initiator and co-chair of a series of SPIE conferences, author or co-author of over 120 publications, and editor or co-editor of 12 *Proceedings of SPIE*.